Journal of Food and Drug Analysis

Volume 30 | Issue 3 Article 9

2022

Composition decipherment of Ficus pumila var. awkeotsang and its potential on COVID-19 symptom amelioration and in silico prediction of SARS-CoV-2 interference.

Recommended Citation

Hu, Hao-Chun; Yu, Szu-Yin; Hung, Xiao-Shan; Su, Chun-Han; Yang, Yu-Liang; Wei, Chien-Kei; Cheng, Yuan-Bin; Wu, Yang-Chang; Yen, Chia-Hung; Hwang, Tsong-Long; Chen, Shu-Li; Szatmári, István; Hunyadi, Attila; Tsai, Yi-Hong; and Chang, Fang-Rong (2022) "Composition decipherment of Ficus pumila var. awkeotsang and its potential on COVID-19 symptom amelioration and in silico prediction of SARS-CoV-2 interference.," *Journal of Food and Drug Analysis*: Vol. 30 : Iss. 3 , Article 9.
Available at: https://doi.org/10.38212/2224-6614.3419

ORIGINAL ARTICLE

Composition decipherment of *Ficus pumila* var. *awkeotsang* and its potential on COVID-19 symptom amelioration and *in silico* prediction of SARS-CoV-2 interference☆

Hao-Chun Hu [a,†], Szu-Yin Yu [b,†], Xiao-Shan Hung [a], Chun-Han Su [c,d], Yu-Liang Yang [c,e], Chien-Kei Wei [a], Yuan-Bin Cheng [f], Yang-Chang Wu [f,g,h], Chia-Hung Yen [a], Tsong-Long Hwang [i,j,k], Shu-Li Chen [a], István Szatmári [l], Attila Hunyadi [b], Yi-Hong Tsai [a,m,**], Fang-Rong Chang [a,f,n,o,*]

[a] Graduate Institute of Natural Products, College of Pharmacy, Kaohsiung Medical University, Kaohsiung 80708, Taiwan
[b] Institute of Pharmacognosy, Interdisciplinary Excellence Centre, University of Szeged, 6720 Szeged, Hungary
[c] Agricultural Biotechnology Research Center, Academia Sinica, Taipei, 115, Taiwan
[d] Research Center for Chinese Herbal Medicine, College of Human Ecology, Chang Gung University of Science and Technology, Taoyuan, 333, Taiwan
[e] Biotechnology Center in Southern Taiwan, Academia Sinica, Tainan, 711, Taiwan
[f] Department of Marine Biotechnology and Resources, National Sun Yat-sen University, Kaohsiung, 804, Taiwan
[g] Graduate Institute of Integrated Medicine, China Medical University, Taichung, 40402, Taiwan
[h] Chinese Medicine Research and Development Center, China Medical University Hospital, Taichung 40402, Taiwan
[i] Graduate Institute of Natural Products, College of Medicine, Chang Gung University, Taoyuan, 33302, Taiwan
[j] Research Center for Chinese Herbal Medicine, Research Center for Food and Cosmetic Safety, and Graduate Institute of Health Industry Technology, College of Human Ecology, Chang Gung University of Science and Technology, Taoyuan, 33303, Taiwan
[k] Department of Anesthesiology, Chang Gung Memorial Hospital, 33305, Taoyuan, Taiwan
[l] Institute of Pharmaceutical Chemistry and ELKH-MTA-SZTE Stereochemistry Research Group, Hungarian Academy of Sciences, University of Szeged, Szeged, Hungary
[m] Department of Pharmacy and Master Program, Collage of Pharmacy and Health Care, Tajen University, Pingtung County 90741, Taiwan
[n] Drug Development and Value Creation Research Center, Kaohsiung Medical University, Kaohsiung, 80708, Taiwan
[o] Department of Medical Research, Kaohsiung Medical University Hospital, Kaohsiung Medical University, Kaohsiung, 80708, Taiwan

Abstract

The jelly from achenes of *Ficus pumila* var. *awkeotsang* (FPAA) is a famous beverage ingredient in Taiwan. In this work, ficumarin (1), a new compound was obtained from its twigs (FPAT) and elucidated with comprehensive spectroscopic data. The biosynthetic origin was proposed from the *p*-coumaroyl-CoA pathway. Alloxanthoxyletin, betulinic acid, and catechin were identified as the major and active constituents responsible for relieving neutrophilic inflammation by FPAT. Among them, the most potent alloxanthoxyletin was found to interact with PRO350 and GLU377 of human INOSOX. Further, Nrf2 activating capacity of the FPAT fraction and its coumarins was confirmed. With the analysis of LC-MS/MS data and feature-based molecular networking, coumarins were found as the dominant and responsible components. Notably, alloxanthoxyletin increased Nrf2 expression by up to 816.8 ± 58% due to the interacting with the VAL561, THR560 and VAL420 residues of 5FNQ protein. COVID-19 Docking Server simulation indicated that pyranocoumarins would promisingly interfere with the life cycle of SARS-CoV-2. FPAT was proven to exert

☆ This article is dedicated to the memory of Prof. Dr. Ferenc Fülöp.

Received 26 November 2021; revised 14 March 2022; accepted 5 June 2022.
Available online 15 September 2022

* Corresponding author at: Graduate Institute of Natural Products, College of Pharmacy, Kaohsiung Medical University, Kaohsiung 80708, Taiwan.
** Corresponding author at: Department of Pharmacy and Master Program, Collage of Pharmacy and Health Care, Tajen University, Pingtung County 90741, Taiwan.
E-mail addresses: lyph0719@hotmail.com (Y.-H. Tsai), aaronfrc@kmu.edu.tw (F.-R. Chang).
† These authors contributed equally.

https://doi.org/10.38212/2224-6614.3419

anti-inflammatory activity on neutrophils and to activate Nrf2, and may likely be developed as a complementary supplement in the treatment of COVID-19 patients.

Keywords: Anti-neutrophilic inflammation, COVID-19, *Ficus pumila* var. *awkeotsang*, Global natural products social molecular networking (GNPS), Nrf2 antioxidative defense system

1. Introduction

The *Ficus* genus (Moraceae), which distributes within tropical to subtropical regions, comprises more than 850 species. *Ficus pumila* var. *awkeotsang* (Makino) Corner (FPA), is one of the subspecies, known as jelly fig, endemically and wildly found in mid-to high-altitude mountains of Taiwan. It was morphologically observed and recorded as a large, evergreen, and scandent shrub. The geographic inhabitation is at altitudes of 800–1900 m in the latitude-longitude grid of 120–122 °E, 22–25°N [1]. FPA is even economically cropped for making a Taiwanese beverage ingredient natively named as "Aiyu jelly". Pectinesterases in "achene of FPA (FPAA, seed cluster)" would be activated during soaking and rubbing FPAA in cold water to de-esterified pectin. Low methoxyl pectin would be further formed as jelly in the presence of calcium ions. Serving FPA (Aiyu) jelly with lemon juice and shaved ice is one of the most popular summer beverage in Taiwan. Moreover, the dried leaves, twigs (FPAT) and syconia of FPA can also be boiled in water to make "FPA tea", which was told to consume for clearing heats. The marketing value of FPA in Taiwan reaches up to 24 million USD annually based on the 705 metric tons of output from just 650 ha of cultivated area. It was regarded as a highly remunerative crop and dedicatedly developed by Taiwan local government [2–4].

FPA was once published in 1904 as a new species named "*F. Awkeotsang* Makino" by a Japanese botanist, Makino Tomitaro. However, it was further confirmed to be a variant of *F. pumila* L (FP), and its scientific name was revised as *F. pumila* L. var. *awkeotsang* (Makino) Coner in 1960. Detailed taxonomic information and the accepted name of FPA has been checked with the authoritative website in Taxonomy[5]: http://www.worldfloraonline.org/. The major differences between FPA and FP can be distinguished by characteristics of their syconia and foliage, geographic distribution, even the specific pollinating fig wasp of each. Shapes of FPA syconia and foliage are obviously longer and thinner than FP. The inhabiting altitude of FP is at the height lower than 500 m which was explicitly in disparity to the FPA of higher than 800 m.

According to literature review, all studies on FPA were focused on the achenes and achene-derived product (FPAA). Since the concept of circular bioeconomy (CBE) is increasingly noticed and becoming a prominent trend [6], the twigs of FPA (FPAT) folksily made as FPA tea can be regarded as an agro-industrial byproduct secondary generated with the annual harvested FPAA. FPAT is a target worthy to be salvaged and developed for value-added agriculture.

Previous research focused on FP, the mother species of FPA, revealed that methanolic extract of the dried FP stems and leaves was proven to exert analgesic and anti-inflammatory properties *in vivo*. Several chemical constituents were identified including apigenin, astragalin, chrysin, genistein, hesperidin, isoquercitrin, luteolin and rutin [7]. However, the evidence of biofunctions and the corresponding chemical constituents from FPAT are still in a mist and may be considered as a fresh land to explore.

Based on our preliminary data, methanolic extract of FPAT (FPATM) exhibited anti-inflammatory and Nrf2 (Nuclear factor erythroid 2-related factor 2) activities (Table S1-S2 (https://www.jfda-online.com/cgi/editor.cgi?article=3419&window=additional_files&context=journal)). The Keap1 (Kelch-like ECH-associated protein 1)-Nrf2 pathway is an important part of cellular defense [8]. The system regulates the production of antioxidants in human body [9]. Previous investigations had revealed that Keap1 inhibitors/Nrf2 activators may enhance the central defensive mechanism against oxidative stress triggered by infectious pathogens, even noticeably including SARS-CoV-2 [10]. These substances may alleviate cytokine storm in COVID-19 patients and reduce the complications for better clinical recovery. Nonetheless, to establish *in vitro* or *in vivo* platforms for evaluating the potential against COVID-19-realted syndromes is a complicated challenge. Molecular docking, which had been conducted to calculate and predict the behavior and affinity within specific moieties of a small molecule and the binding sites of a target protein responsible for bioactivity, is now a popular computational screening approach [11]. With diversely developed software, platforms and docking strategies, druggability of lead compounds can be further designed

and optimized. It is a promising *in silico* tool extensively used in the entire drug discovery field and pharmaceutical academia and industry.

In this study, we have carried out a complete work to isolate and identify chemical constituents of FPATM through bioactivity-guided separation for revealing those responsible for Nrf2 and anti-neutrophilic inflammatory activities. These two biological responses are crucial in the lethal complications on COVID-19 patients. To elaborate relationships between chemicals and bioactive targeted proteins, we utilized a software, Discovery Studio® (DS®), and a platform, Achilles Blind Docking Server (http://bio-hpc.ucam.edu/webBD/index.php/entry), to clarify their binding affinities.

Furthermore, isolates were subjected to COVID-19 Docking Server which is a meta-platform built up for unveiling the interfering capacity in the life cycle of SARS-CoV-2 [12]. Additionally, the partitioned bioactive fraction was analyzed by Global Natural Products Social Molecular Networking (GNPS), a world wide web-based fragmentation mass spectrometry database (MS/MS) [13]. A comprehensive investigation of the constitutions and bio-functional potential of FPATM is herein reported.

2. Materials and methods

2.1. Plant material

The twigs of *F. pumila* var. *awkeotsang* (FPA) were collected in Pingtung City, Taiwan in August, 2016. The raw plant material was identified by Professor Fang-Rong Chang. A voucher specimen (code no. KMU-FPA001) was stored in the Graduate Institute of Natural Products, College of Pharmacy, Kaohsiung Medical University. The detailed information of FPATM extraction, procedures for the isolation and physical data of compound **1**, protocols of bioassays and preliminary data are provided in the supporting information.

2.2. In silico calculation

Possible absolute stereostructures of **1**, the minimized energy conformers, were optimized in the Molecular mechanics (MM2) calculations. These 3D structures were outputted as xyz type files to be calculated through MMFF94 force field program (Spartan 16 software, Wavefunction Inc.; Irvine, CA, U.S.A.) for their conformational results. These possible conformers were submitted into Gaussian 09 software (Gaussian Inc.; allingford, CT, U.S.A.), optimized in the methodology of time-dependent density functional theory at the B3LYP/6-31+G(d,p) level, and then calculated using the GIAO-DFT at the B3LYP/6-311+g(2d,p) level for SOR. Both levels were simulated in MeOH solvent phase. These possible absolute results were submitted to the GIAO-DFT at the mpw1pw91/6-311+g(2d,p) level for NMR. The calculated and experimental NMR data were analyzed by DP4 methods. The absolute structure of **1** were further computed with ECD spectrum at the B3LYP/6-311++G(d,p) level in the MeOH solvent phase [14,15].

2.3. Molecular docking methods

Discovery Studio (DS®) is a software suite for predicting the molecular interactions between the target receptor and ligand molecule in 3D space. Achilles Blind Docking Server is a platform which approach was used for docking small molecule to the target protein but without any effort or prior knowledge using in the platform. COVID-19 Docking Server is a specific platform only severing for docking small molecule, peptide, or antibody to COVID-19 protein targets.

2.4. LC-MS/MS analysis

Mobile phase A consisted of 0.1% formic acid in deionized water, and mobile phase B comprised 0.1% formic acid in acetonitrile. Gradient elution was as follows: 95% A at 0 min; 0.5% A at 6 min; 0.5% A at 8 min; 95% A at 8.2 min; and 95% A at 10 min. The flow rate was kept at 0.4 mL/min, column temperature was set to 40 °C, and injection volume was 10 μL. The Orbitrap Elite mass spectrometer equipped with HESI ion source (Thermo Fisher Scientific, USA) was used as a detector. MS was operated in positive ion and negative ion mode with *m/z* range 100–1500 for MS1 and 50–1500 for MS2. Top 4 most intense precursors were selected for fragmentation in data-dependent acquisition (DDA) analysis. The collision energy used for fragmentation was set to 35 (arbitrary unit).

2.5. Feature-based molecular network

Feature-Based Molecular network (FBMN) was generated by counting the similar of MS2 spectrum of different edges with cosine score above 0.7. The precursor and fragment ion mass tolerance were set at 0.02 Da. The merge program was set the ppm and RT tolerance as 20 ppm and 0.15 min, respectively. The spectra data in FBMN were searched against GNPS spectral libraries and isolated compound standards. All matching structures which were drew

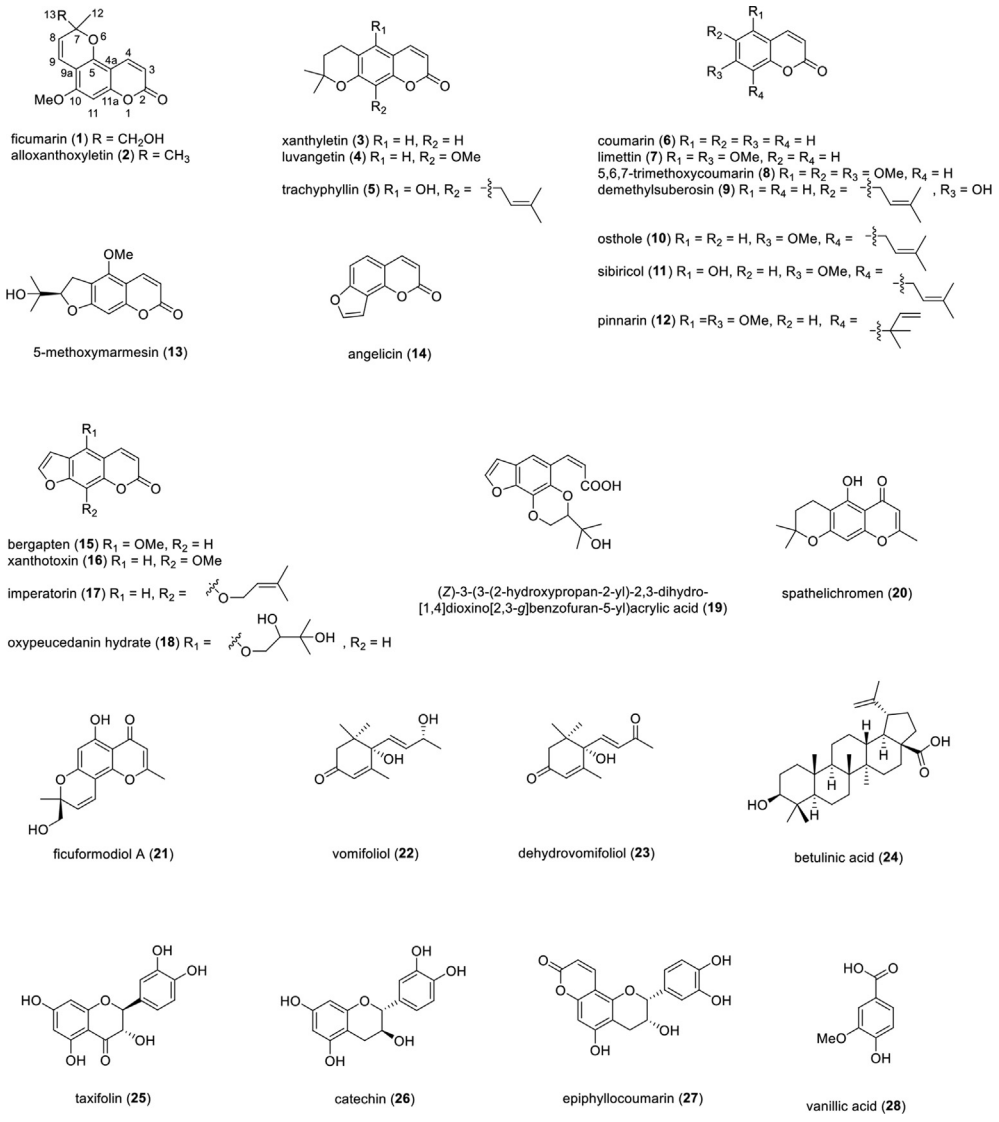

Fig. 1. Structures of compounds 1–28 isolated from FPATM.

in FBMN spectrum were required to have a score above 0.8.

3. Results

3.1. Preliminary screening of the bioactivities of FPATM fractions

The cytotoxic properties of FPATM were tested against three cancer cell lines, including HepG2 (human liver hepatocellular carcinoma), A549 (human lung carcinoma), and MD-MBA-231 (human breast adenocarcinoma). It showed no cytotoxicity on these cancer cells (Table S3 (https://www.jfda-online.com/cgi/editor.cgi?article=3419&window=additional_files&context=journal)). In the evaluation of anti-neutrophilic inflammation, FPATM exhibited notable potential in inhibiting superoxide anion generation and elastase release (Table S1 (https://www.jfda-online.com/cgi/editor.cgi?article=3419&window=additional_files&context=journal)). The partitioned 75% $MeOH_{(aq)}$ layer of FPATM (FPATM-75) showed significant Nrf2 activity in HaCaT cells (human immortalized keratinocytes) (Table S2 (https://www.jfda-online.com/cgi/editor.cgi?article=3419&window=additional_files&context=journal)).

*Table 1. ^{1}H and ^{13}C NMR Data of **1** [a] in $CDCl_3$.*

Position	δ_H, mult (*J* in Hz)	δ_C, type
1		
2		161.5, C
3	6.14, d (9.6)	111.6, CH
4	7.92, d (9.6)	138.4, CH
4a		103.6, C
5		150.0, C
6		
7		81.1, C
8	5.53, d (10.1)	123.7, CH
9	6.77, d (10.1)	118.8, CH
9a		106.4, C
10		158.5, C
11	6.33, s	92.0, CH
11a		156.1, C
12	1.41, s	23.0, CH_3
13	3.72, d (11.9)	68.8, CH_2
	3.68, d (11.9)	
10-OMe	3.86, s	56.1, CH_3

[a] ^{1}H and ^{13}C NMR data (δ) were measured at 400 and 100 MHz, respectively; Chemical shifts are in ppm.

3.2. Compounds purified and identified from FPATM

In this study, one new and 28 known compounds were isolated from FPATM. These were identified as coumarins (**1**–**19**), chromens (**20** and **21**), sesquiterpenoids (**22** and **23**), a triterpenoid (**24**), flavonoids (**25**–**27**) and a benzoic acid derivative (**28**). The isolated coumarins can further be classified into different sub-types, i.e., pyranocoumarin-angular (**1**–**2**), pyranocoumarin-linear (**3**–**5**), coumarin (**6**–**12**), dihydrofuranocoumarin (**13**), furanocoumarin-angular (**14**), furanocoumarin-linear (**15**–**19**), and chromen (**20**–**21**) derivatives. The structures of all isolates (**1**–**28**) are illustrated in Fig. 1.

Ficumarin (**1**) was obtained as a colorless oil; the ^{1}H NMR and ^{13}C NMR data are presented in Table 1. Based on the 2D NMR, the ^{1}H-^{1}H COSY signals revealed two fragments of H-3 (δ_H 6.14)/H-4 (δ_H 7.92) and H-8 (δ_H 5.53)/H-9 (δ_H 6.77). The angular type pyranocoumarin moiety was revealed by the key HMBC correlations between H-3/C-2, C-4a, H-4/C-2, C-5, C-11a, H-8/C-7, C-9a, H-9/C-5, C-7 and H-11/C-4a, C-9a, C-10, C-11a. The HMBC cross-peak of 10-OMe/C-10 revealed the linkage of C-10 and OMe. Further, the relevant H-12/C-7, C-8, C-13, H-13/C-7, C-8 HMBC cross-peaks revealed that H-12 and H-13 are linked on C-7.

Table 2. SOR values.

Exp. 1[a]	−82
Cal. 1a-*R*	−57
Cal. 1a-*S*	57
Cal. 1b-*R*	17
Cal. 1b-*S*	−17
Cal. 1c-*R*	−44
Cal. 1c-*S*	44

[a] $[\alpha]_D^{22}$ (*c* 0.05, MeOH)

In accordance with the 1D and 2D NMR data, three possible constitutional isomers may be proposed as the structure of compound **1**, viz. **1a**, **1b**, and **1c** (Fig. S7). All possible structures contain one chiral center, therefore representing six possible absolute configurations such as **1a-*S***, **1a-*R***, **1b-*S***, **1b-*R***, **1c-*S***, and **1c-*R*** (Fig. S8). The specific optical rotations (SOR) of these isomers were calculated as follows: The experiment SOR of **1** was −82°, and the calculated SOR values for **1a-*R***, **1b-*S***, and **1c-*R*** were negative, and for **1a-*S***, **1b-*R***, and **1c-*S*** were positive (Table 2). According to the comparison of experimental data with calculated SOR of **1**, isomers **1a-*R***, **1b-*S***, and **1c-*R*** remained as possibilities.

The quantum-chemical calculations of ^{13}C NMR chemical shifts were performed to identify the structures of **1a-*R***, **1b-*S***, and **1c-*R*** (Fig. 2a). The correlation coefficients (R^2) of **1a-*R***, **1b-*S***, and **1c-*R*** were 0.9875, 0.9944, and 0.9974, respectively (Fig. 2b). The individual deviations between the predicted and experimental ^{13}C NMR chemical shifts for **1c-*R*** were less than 5.0 ppm, except for that of C-2, C-3, and C-8 around 6 ppm (Fig. 2c). The calculated ^{13}C NMR chemical shifts of **1c-*R*** showed an excellent match with the experimental data with a correlation coefficient (R^2) = 0.9974 (Fig. 2b). Steps using the DP4 parameter to confidence level for NMR assignment, in the structure **1c-*R*** shows a 100.0% match. As stated above, only the calculated ^{13}C NMR chemical shifts and DP4 results of **1c-*R*** matched with the experimental ^{13}C NMR data.

To decide the absolute configuration of **1**, quantum-chemical electronic circular dichroism (ECD) calculations were performed. Enantiomers **1c-*S*** and **1c-*R*** were subjected to a time-dependent density functional theory (TDDFT) calculation at the B3LYP/6-311++G(d,p) level. Ultimately, the calculated ECD curve of **1c-*R*** matched with the experimental ECD curve, but the **1c-*S*** was contrary (Fig. S9). Combining all the evidence, the absolute configuration of **1** was assigned as **1c-*R***, and the compound was given the trivial name ficumarin (**1**). The above-described elucidation of compound **1** provides a model, which may help other researchers in the determination for three types of pyranocoumarins in their planar constitution as well as stereochemistry.

The biosynthesis of **1** is proposed to originate from *p*-coumaroyl-CoA. This would first be oxidized to form 2,4-dihydroxycinnamoly-CoA

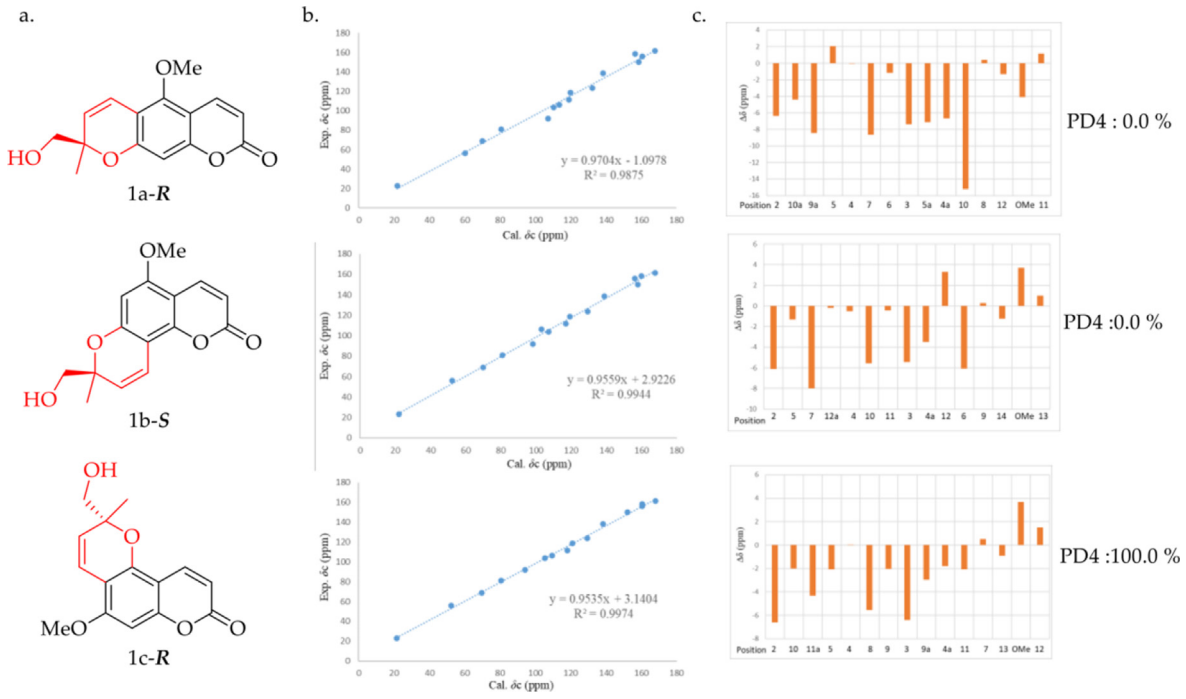

*Fig. 2. ^{13}C NMR calculation and DP4 results of three possible structures of **1**. (a) Structures of **1a-R**, **1b-S**, and **1c-R**. (b) Linear correlation between predicted and experimental ^{13}C NMR chemical shifts of **1a-R**, **1b-S**, and **1c-R**. (c) Individual deviations between the calculated and experimental ^{13}C chemical shifts.*

followed by the spontaneous formation of herniarin. With further oxidation and methylation, herniarin would be transformed to isoscopoletin. Prenylation of isoscopoletin to 5-demethyltoddaculin and oxydation to intermediate A would allow the ring closure to intermediate B. Subsequent dehydration and oxidation of intermediate B are proposed as the final steps to the formation of ficumarin (**1**) (Fig. 3).

3.3. Anti-neutrophilic inflammation activities

Neutrophils play an important role in necroinflammation of COVID-19 patients. Clinical features, such as acute respiratory distress, neutrophilia, and cytokine storm, along with severe inflammatory response syndrome are neutrophil related or caused lethal syndromes [16]. Pathological evidence indicates that neutrophil dysregulation and oxidative

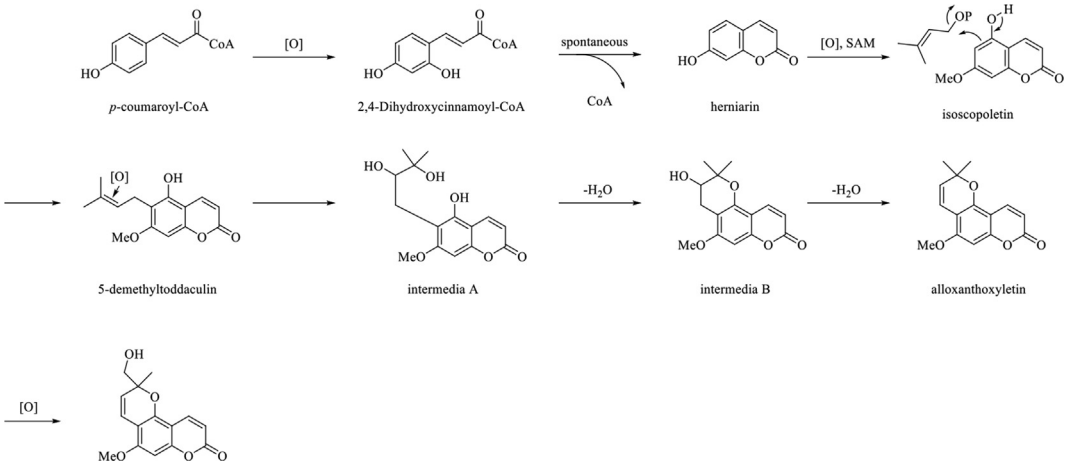

*Fig. 3. Putative biosynthetic pathway of ficumarin (**1**).*

Table 3. Inhibitory effects of isolates on superoxide anion generation in fMLF/CB-induced human neutrophils.

Compounds from FPAT	Superoxide anion generation (μM)[a]
2	5.26 ± 0.58
24	0.51 ± 0.02
26	2.27 ± 0.20

[a] Concentration necessary for 50 % inhibition (IC_{50}).

stress are key factors which cause NET (neutrophil extracellular trap) formation and need to be cleared [17]. To evaluate related bioactivities, all the isolated compounds were assessed in anti-neutrophilic inflammatory evaluations. Alloxanthoxyletin (**2**) showed considerable inhibitory activity on superoxide anion generation from fMLF/CB induced neutrophils (IC_{50} = 5.26 ± 0.58 μM). Moreover, compounds **24** and **26** exerted valuable potential as well (Table 3). According to the results, three FPAT constituents may be responsible for preventing the oxidative stress brought by cytokine storm of necroinflammation in COVID-19 patients.

3.4. Molecular docking of iNOS

Since NO, produced by constitutive nitric oxide synthases (NOS) known as an inducible NOS (iNOS), is a crucial factor in neutrophilic inflammation, the possible involvement of iNOS in the bioactivity of compound **2** was studied. To this, molecular docking was performed with human inducible nitric oxide synthase (INOSOX, PDP: 3E7G) and compound **2** by the Discovery Studio (DS®) software. DS® was conducted to simulate the molecular interactions (binding affinity) between target receptor and the ligand molecule of inflammation.

The results of docking calculations predicted that compound **2** binds to the active site of human INOSOX, to the residue PRO350 (3.07957, 2.64686) by two hydrogen bonds, and to the residue GLU377 (3.81200) by an electrostatic bond (Fig. 4a). The CDOCKER energy, CDOCKER interaction energy, and binding energy of compound **2** with 3E7G were −10.904, −24.9855, and −58.8654, respectively.

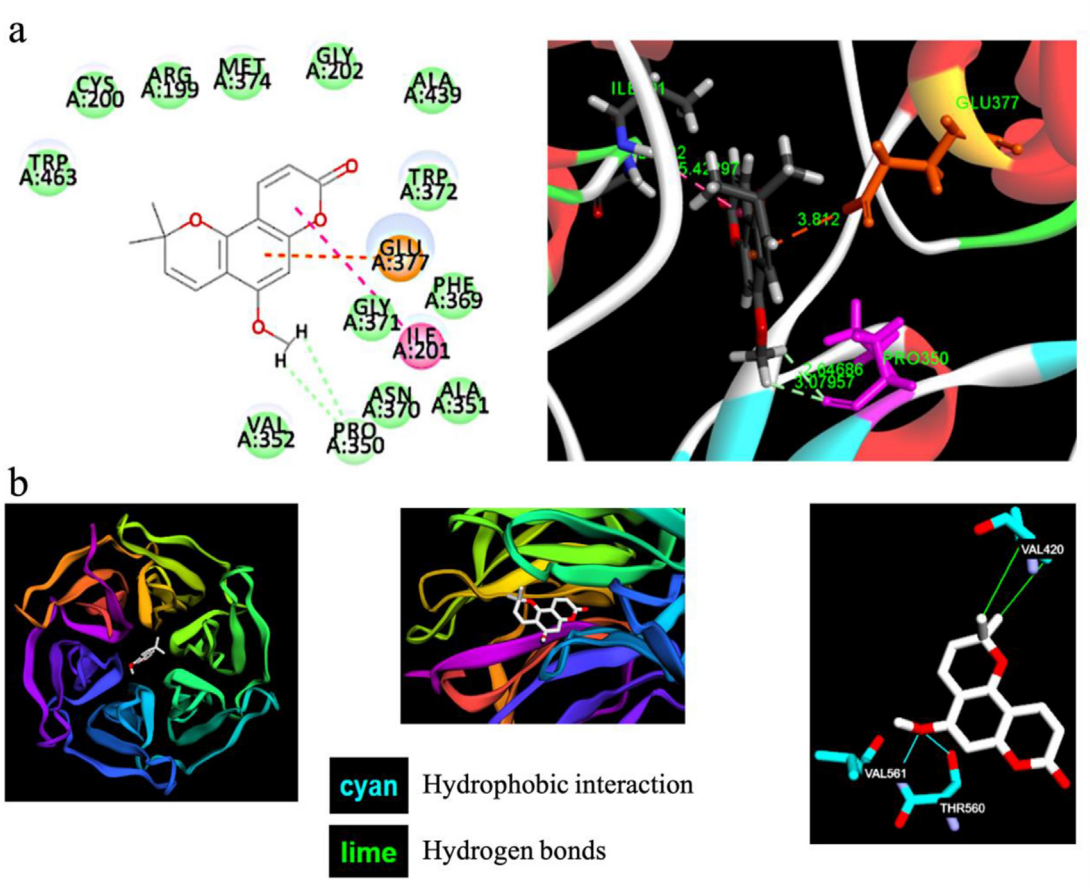

Fig. 4. (a) Docking models of human INOSOX in complex with compound 2; (b) The predicted docking node of compound 2 in 5FNQ, and the residues interacting with compound 2.

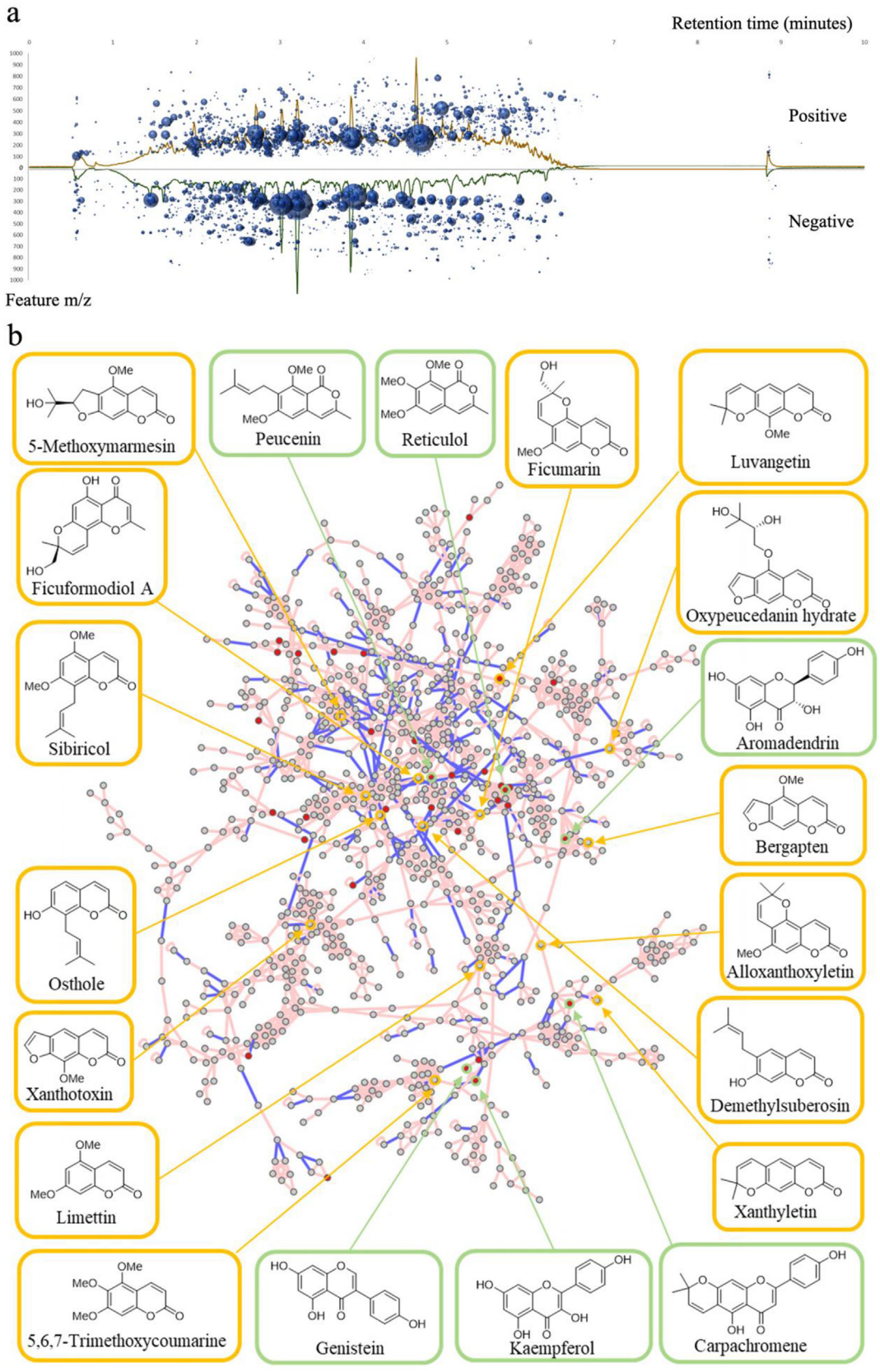

Fig. 5. (a) Mirror plot of FPATM-75 in LC-MS/MS. The upper (yellow line) and downer (green line) panels show results obtained in positive and negative mode, respectively. The blue sphere sizes represent peak heights from MS/MS data. The x-axis shows retention time (minutes) of components in LC, and the y-axis shows the m/z values for both ionization modes; (b) FBMN of polyketide pathway-rich cluster. Yellow frames mark the isolated compounds. Green frames mark matched database compounds. The blue edges show observed links between positive mode and negative mode data.

Table 4. Nrf2 activity of isolated compounds.

compounds	Nrf2 activation in HacaT cell (%, mean ± SD)[a]	compounds	Nrf2 activation in HacaT cell (%, mean ± SD)[a]
1	105.8 ± 0.5	**14**	340.6 ± 29
2	**816.8 ± 58**	**15**	238.4 ± 22
3	282.8 ± 31	**16**	177.8 ± 34
4	343.8 ± 23	**17**	771.2 ± 49
5	572.1 ± 34	**18**	107.5 ± 2.0
6	276.8 ± 50	**19**	165.7 ± 5.4
7	163.8 ± 10	**20**	585.2 ± 151
8	286.9 ± 37	**21**	95.5 ± 3.2
9	467.0 ± 59	**22**	100.5 ± 1.6
10	493.1 ± 95	**23**	99.2 ± 4.5
11	282.2 ± 13	**25**	93.8 ± 2.6
12	161.4 ± 13	**28**	95.7 ± 3.2
13	91.0 ± 5.9		
tBHQ[b]	1608.9 ± 46.5		

[a] HacaT, a normal skin cell line. The drug concentration is 10 μM.
[b] TBHQ, 2-(1,1-Dimethylethyl)-1,4-benzenediol, was used as positive control for Nrf2 activation. The drug concentration is 10 μM.

3.5. GNPS analysis focused on the FPATM fractionate with Nrf2 activity

Molecular networking (MN) is a visualization approach to present the chemical space in accordance with outcomes obtained from tandem mass spectrometry (MS/MS) experiments. The concept of MN application was to evaluate structural similarities between analyzed metabolites and the linked worldwide sharing and co-building database (GNPS). The communications are based on the MSn fragmentation spectrum of under test compounds to compare with plenty of previously created information. This technique is particularly utilized on high throughput chemical analyses of natural products [18].

Since the FPATM-75 was found exerting promising Nrf2 activating capacity, this fraction was measured and displayed with positive and negative mode of LC-MS/MS (liquid chromatography coupled with tandem mass spectrometry) data as a mirror plot (Fig. 5a). Sizes of blue spheres are presented to express the relativities of peak heights and pseudo molecular weights. The observed results indicated that almost all the major components are in the *m*/*z* range of 200–400. Additionally, these LC-MS/MS results were also merged in the GNPS with feature-based molecular networking (FBMN) as well (Fig. 5b).

According to the fragmentation data combined with information from the mirror plot and FBMN, the FPATM-75 was proved to comprise of a wide variety of components biosynthesized through polyketide pathway, i.e., coumarins, isocoumarins, flavanones, and isoflavones. It is worth noting that coumarins were the most abundant constituents isolated from this active fraction.

3.6. Bioactivities on Nrf2

The transcription factor, Nrf2, is a master regulator in cellular oxidation response and inflammation. The activation of Nrf2 is considered as a first-line therapeutic target of related chronic diseases, such as neurodegenerative, cardiovascular, and metabolic diseases [19]. All isolated compounds, except for **24**, **26**, and **27** due to the limited amounts, were subjected to estimate the Nrf2 responses of activation in HacaT cells. Alloxanthoxyletin (**2**), trachyphyllin (**5**), imperatorin (**7**), demethylsuberosin (**9**), osthole (**10**), and spathelichromen (**20**) were tested active with high to moderate levels on Nrf2 in HaCaT cells (Table 4). All these active compounds are FPAT coumarins.

3.7. Molecular docking of Nrf2 activation

Results from Table 4 indicated that compound **2** induced Nrf2 promotion up to 816.8 ± 58%. Therefore, compound **2** was selected for further evaluations by molecular docking. The molecular docking of compound **2** was subjected into Achilles Blind Docking Server and Keap1-Kelch domain (PDB: 5FNQ) was chosen as target receptor referenced from the previous report [20]. The docked pose with the lowest binding energy is shown in Fig. 4b. According to the docking results, compound **2** formed two hydrogen bounds with Val561 and Thr560, along with hydrophobic interaction with Val420.

Table 5. Covid-19 Docking Server results of isolated coumarins

Score Value (kcal/mol)

Protein	Compound																					Total Score Value of Protein
	1	2	3	4	5	6	7	8	9	10	11	12	13	14	15	16	17	18	19	20	21	
Main protease (Mpro)	−7	−7	−6.8	−7.1	−7.9							−6.7				−7.2	−7.3		−7.1	−7.1		−71.2
Papain-like protease	−7.5	−7.5	−7.4	−7.9	−8.2							−7.5				−7.4	−7.4		−7.9	−7.9		−76.6
Nsp3 (207-379, AMP site)	−7.1	−7	−7.2	−7	−7.6			−7		−7.1						−7.4	−7.3		−7.7			−72.4
Nsp3 (207-379, MES site)	−7.9	−7.6	−8	−7.8	−7.8			−7.9						−7.5	−7.4				−8.6	−7.8		−78.3
RdRp with RNA			−9.6		−8.8			−8.8	−8.5			−9.3		−8.4		−8.9	−9	−8.4	−10			**−89.7**
RdRp without RNA	−6.7	−6.8	−7		−7.4							−6.9			−6.8	−7.5	−6.9		−6.8	−6.8		−69.6
Helicase NCB site	−6.8	−6.9	−6.8	−7.1	−7.4							−7.1				−7.1	−7.2		−7.4	−7.1		−70.9
Helicase ADP site	−6.1	−6.1	−6.1	−6.5	−6.4							−6.3				−6.1	−6.2		−6.4	−6.5		−62.7
Nsp14 (ExoN)	−6.4	−6.7	−6.4	−6.4	−7			−6.6								−6.7	−7.1	−6.7	−6.7			−66.7
Nsp14 (N7-MTase)	−8.4	−8.8	−8.8	−8.4	−8.9											−8.5	−8.3	−8.7	−8.3	−8.4		**−85.5**
Nsp15 (endoribonuclease)		−6.6	−6.8	−7.4	−6.6			−7.1				−6.9	−6.6				−6.6		−7.5	−7.4		−69.5
Nsp16 (GTA site)	−7.2	−7.6	−7.3	−7.6	−7.7											−7.7	−7.8	−7.2	−7.4	−7.6		−75.1
Nsp16 (MGP site)		−6.6	−6.8	−6.9	−6.7			−6.7				−6.5					−6.5	−6.5	−7.1	−6.9		−67.2
Nsp16 (SAM site)	−7.1	−7.6	−7.6	−7.6	−7.2			−7.2				−7.1					−7.6		−7.7	−7.6		−74.3
N protein NCB site	−7.7	−7.6	−7.7	−8	−7.7			−7.4				−7.5			−7.8				−8	−8		−77.4
Total point	−86	−100	**−110**	−96	**−113**	0	0	−59	−8.5	−7.1	0	−72	−6.6	−16	−22	−75	−95	−38	**−115**	−89	0	

RF Score Value

Protein	Compound																					Total RF Score Value of Protein
	1	2	3	4	5	6	7	8	9	10	11	12	13	14	15	16	17	18	19	20	21	
Main protease (Mpro)	5.5	5.3	5.5	5.7	6.1							5.4				5.9	5.7		5.4	5.7		56.2
Papain−like protease	6	6	6.1	6.1	6.1							5.6				6.1	5.7		6.2	6.1		60
Nsp3 (207-379, AMP site)	5.5	5.7	5.5	4.8	5.5			5.2		5.2						5.7	6		5.5			54.6
Nsp3 (207-379, MES site)	5	4.7	4.6	5.8	5.7			4.6						4.5	4.4				5.8	5.8		50.9
RdRp with RNA			6.6		6.1			6.3	6.2			6		5.6		6.3	6.2	6.5	6.8			**62.6**
RdRp without RNA	4.8	4.7	6.3		5.7							4.5			3.8	5.3	5.5	4.4	4.4			49.4
Helicase NCB site	4.9	4.8	4.9	5.3	5.7							5.3				5.6	5.4		5.1	5.3		52.3
Helicase ADP site	3.7	3.7	3.9	3.9	5.5							4.6				4.3	4.4		4.1	3.9		42
Nsp14 (ExoN)	4.5	4.2	4.5	4.1	5.5			4.4								4.8	5.6	5.3	4.5			47.4
Nsp14 (N7-MTase)	6	6.2	4.9	6.3	6.5											6	6.1	6.1	5.9	6.3		**60.3**
Nsp15 (endoribonuclease)		4.4	4.2	4.4	5.4			4.8				4.8	4.4				5.3		4.6	4.4		46.7
Nsp16 (GTA site)	4.1	4	4.7	4.8	5.3											5.2	5.6	5	4.3	4.8		47.8
Nsp16 (MGP site)		4	4.1	3.8	4.7			4.4				4.2					4.6	4.9	4.2	3.8		42.7
Nsp16 (SAM site)	4.1	3.9	5.2	4.7	5.8			4.9				5					5.6		5.5	4.7		49.4
N protein NCB site	4.7	4.9	4.9	5.5	5.7			5.1				4.8			3.8				5.1	5.5		50
Total point	59	67	**76**	65	**85**	0	0	40	6.2	5.2	0	50	4.4	10	12	55	72	32	**77**	56	0	

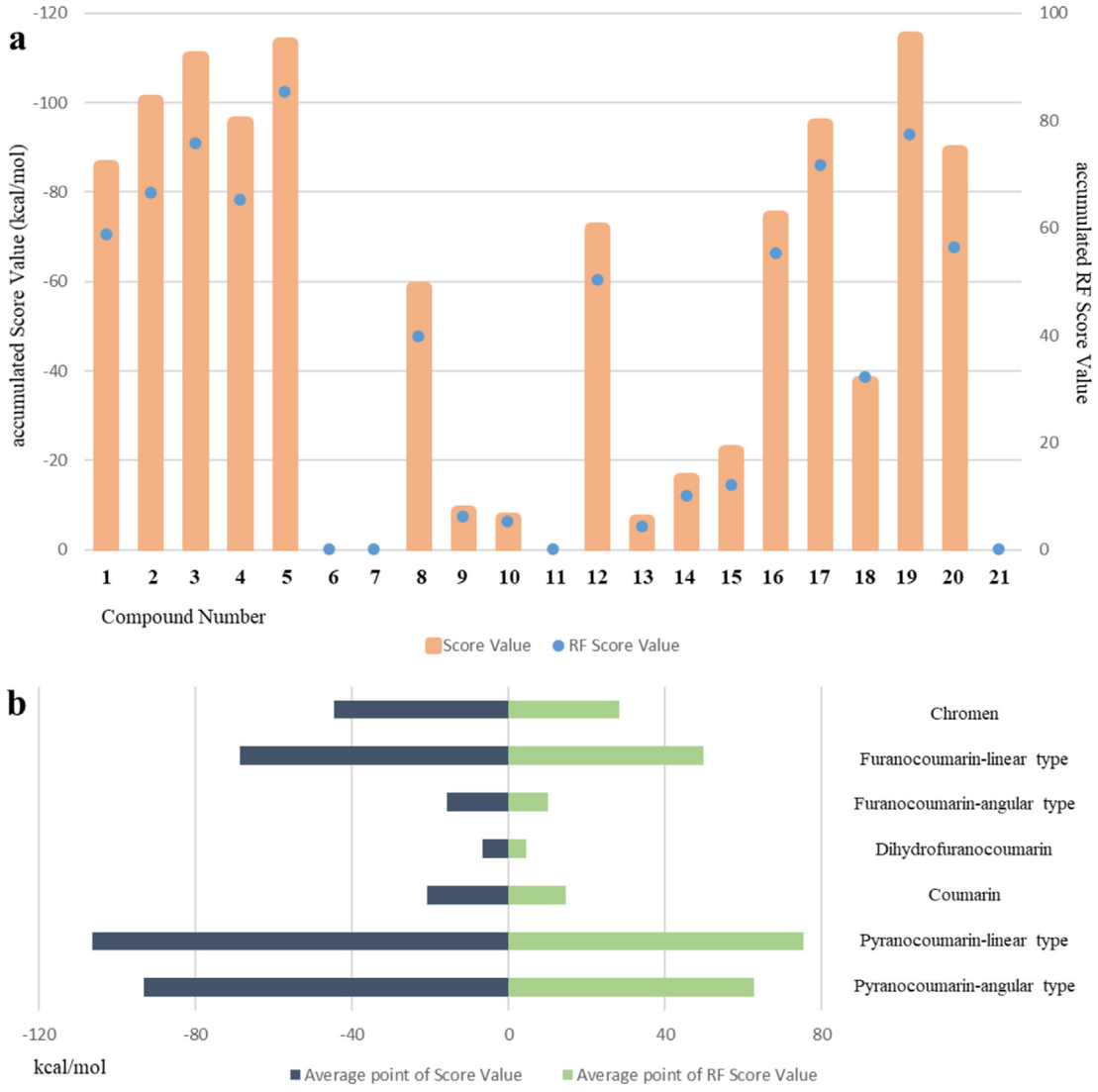

Fig. 6. (a) Accumulated score for isolated coumarins; (b) Average scores in different types of coumarins.

The lowest binding energy score between compound **2** and 5FNQ was −6.40 kcal/mol.

3.8. In silico investigation of FPAT coumarins in Nrf2 antioxidative defense system and COVID-19

Since December 2019, an outbreak of severe acute respiratory syndrome coronavirus 2 (SARS-COV-2) pandemic has been occurring as a worldwide disaster. It was named as coronavirus disease-2019 (COVID-19), 2,201,564 patients (confirmed cases) and caused which had infected 536,590,224 patients (confirmed cases) and caused 6,316,655 deaths recorded till 2022/06/15 (https://covid19.who.int/). The case numbers are continuously accumulating everyday [21,22]. Lethal symptoms of COVID-19 are mostly recognized with the incidence of acute respiratory distress syndrome (ARDS) and pneumonia. The excessive production of inflammatory cytokines, so-called cytokine storm, during the severe stage of COVID-19 progression, leads to widespread tissue damage, multi-organ failure and death. These pathological roles have been linked to the mortality of COVID-19 patients [23].

It's noteworthy that symptoms of cytokine storm in COVID-19 can be counteracting via the antioxidative defense mechanisms in the body. To enhance the production of biological antioxidants, balance of the Keap1-Nrf2 system plays a crucial role *in vivo*. Nrf2 must be released from the Keap1-Nrf2 protein complex to stimulate the antioxidant response element (ARE) present in the antioxidant genes. Activating agents of Nrf2 have been reported

to potentially serve as adjunct therapy to manage cytokine storm against the rapidly deteriorated condition in COVID-19 patients [10].

Coumarins had previously been demonstrated to activate Nrf2 signaling in different cellular and animal models, which would make them have a potential as autogenous antioxidant and anti-inflammatory agents. Furthermore, coumarins were demonstrated by molecular docking approaches to bind with Keap1, which might interfere with the Keap1/Nrf2 interaction and therefore indirectly contribute to the activation of Nrf2 [24]. Additionally, natural coumarins have been suggested as potential anti-SARS-CoV-2 agents based on docking studies [25].

COVID-19 Docking Server (https://ncov.schanglab.org.cn/), which is an online meta server, was built for elaborating the SARS-CoV-2 target–ligand interactions. Structures of proteins involved in the virus life cycle were established based on the homologs of coronavirus. Through this server, the binding mode and affinity between estimated molecules and target protein can be deduced. Moreover, batch docking mode in this server is especially provided for exploring the changes within a set of small molecules and various of their chemical substitutions based on the predicted binding intensities. In one batch docking, the top 10 models would be ranked by the assessed binding energies and RF-scores, which is a machine learning approach to display the predicted affinity of protein-ligand binding [12].

Based on the above, all the isolated coumarin type components from FPAT, including the new coumarin **1** as well as known coumarins **2**–**19** and chromens **20** and **21**, were submitted into COVID-19 Docking Server for unveiling their interfering capacity in the life cycle of SARS-CoV-2 virus. Docking results of the top ranked 10 compounds in difference proteins expressing as Score Value (kcal/mol), RF Score Value and their total point (accumulated score, sum) are presented in Table 5 and Fig. 6a. Altogether, xanthyletin (**3**), trachyphyllin (**5**), and (*E*)-3-(3-(2-hydroxypropan-2-yl)-2,3-dihydro-[1,4]dioxino[2,3-*g*]benzofuran-5-yl)acrylic acid (**19**) were promising ones in all simulations. In all the simulated ligan-protein docking model, RNA-dependent RNA polymerase (RdRp) and C-terminal guanine-N7 methyl transferase (N7-MTase), nonstructural protein 14 (Nsp14) displayed higher score than all other proteins. The C-terminal domain functions played a N7-MTase for mRNA capping. The active site of Nsp14 was defined as the SAH binding site (PDB code: 5C8S). RdRp with RNA in the COVID-19 Docking Server was a complex with RNA and triphosphate form of Remdesivir (RTP) which was the same as the PDB bank database with code of 7BV2. N7-MTase and Nsp14 were important for viral replication and transcription in coronaviruses.

According to the calculated averaging points of Score Value and RF Score Value visualized in Fig. 6b, not only the linear pyranocoumarins but also the angular ones exhibited high average docking scores. These outcomes provided an *in silico* evidence and indicated that linear coumarins may be an advanced promising type of lead compounds in natural coumarins against SARS-CoV-2.

4. Discussion

FPAT, twigs of *F. pumila* var. *awkeotsang*, has extensively been utilized as a "folk" supplement offering health benefits. From this herbal drug, a new compound (**1**) was isolated and its structure was elucidated in detail for the first time. The established model in the determination of various possible constitutions and stereochemistry of pyranocoumarins may help other scientists in determination of related structures in the future. Compound **1** is biosynthesized from the precursor of *p*-coumaroyl-CoA.

Alloxanthoxyletin (0.12%), betulinic acid (1.10%) and catechin (1.27%) are major and active components from FPAT exerting anti-inflammatory activity on neutrophils. Alloxanthoxyletin (**2**) is a coumarin-type compound and the most potent constituent (IC_{50} = 5.26 ± 0.58 μM) in FPAT. Molecular docking simulations revealed that the most potent coumarin, alloxanthoxyletin, binds to the PRO350 and GLU377 residues of the human INOSOX protein. The Nrf2 activating capacity of the 75% $MeOH_{(aq)}$ fraction of FPATM (FPATM-75) was found, and this fraction was further analyzed by LC-MS/MS. Through feature-based molecular networking (FBMN), FPATM-75 was proven to comprise coumarins, isocoumarins, flavanones, and isoflavones, among which coumarins are the dominant components. FPAT coumarins, alloxanthoxyletin, imperatorin, trachyphyllin, demethylsuberosin, osthole and spathelichromen, were tested active and responsible for activating the Nrf2 antioxidative defense system in HaCaT cells. Especially, alloxanthoxyletin triggered the Nrf2 by up to 816.8 ± 58% owing to construct hydrogen bonds with VAL561 and THR560, and hydrophobic interaction with VAL420 in the Keap1-Kelch domain. Coumarins from FPAT with inhibitory activity on neutrophilic inflammation and simultaneously activating Nrf2 may enhance central

defensive mechanism against oxidative stress, cytokine storm and necroinflammation occurring in COVID-19 patients.

According to the computational calculations from COVID-19 Docking Server, FPAT coumarins like pyranocoumarins (**1**–**5**) and R_2 substituted furanocoumarins (e.g., **16**, **17**, and **19**) may be considered as promising lead compounds in interfering with the life cycle of SARS-CoV-2 virus.

FPAT was proven to not only inhibit anti-neutrophilic inflammation and activate Nrf2, but also have the potential in stopping the virus through target - ligand interactions by specific FPAT coumarins. This may lead to the conclusion that FPAT may be developed as a complementary supplement in alleviating severe syndromes caused by SARS-CoV-2 infection.

Conflict of interest

The authors declare that they have no known competing financial interests or personal relationships that could have appeared to influence the work reported in this paper.

Acknowledgement

This research was funded by the Ministry of Science and Technology, Taiwan awarded to F.-R. Chang, grant number: MOST 108-2320-B-037-022-MY3, 109 -2927-I-037 -502, 106-2811-B-037-025, 110-2811-B-037 -518. In addition, this research was partially funded by the Drug Development and Value Creation Research Center of Kaohsiung Medical University; Department of Medical Research of Kaohsiung Medical University Hospital awarded to F.-R. Chang (grant number: KMU-TC108A03-11 and KMU-TC108A03-4). A. H. acknowledges the NKFIH, Hungary (grant number: K-134704). We would like to specially thank to the Center for Research Resources and Development (CRRD) of Kaohsiung Medical University for providing the assistance in NMR, LC-MS and GC-MS are sincerely appreciated as well.

References

[1] Li HL, Liu TS, Huang TC, Koyama T, Charles CE. Ficus pumila var. awkeotsang (Makino) Corner. In: Flora of Taiwan editorial committee; U.S.-R.O.C. cooperative science program (Eds.), Flora of Taiwan (1st ed.). 2; 1975-1979. p. 145.

[2] Jiang CM, Lai YJ, Lee BH, Chang WH, Wu MC, Chang HM. Changes in physico-chemical properties of pectin from jelly fig (*Ficus awkeotsang* Makino) seeds during extraction and gelling. Food Res Int 2002;35:31–5.

[3] Jiang CM, Lai YJ, Chang WH, Wu MC, Chang HM. Pectinesterase inhibitor in jelly fig (*Ficus awkeotsang* Makino) achenes. J Food Sci 2006;66:225–8.

[4] Lu MC, Liu IC, Sun CL. Cultivation and environmental ecology of aiyuzi, an endemic species in Taiwan. In: Ting ST, Shen Y, Wu CL, Wu RC, Lin MF, Lu HS, editors. Agricultural biotechnology industry quarterly. Biotechnology industry study centre. 59. Taiwan: Taiwan institute of economic research; 2019. p. 27.

[5] WFO: World Flora Online. *Ficus pumila* var. awkeotsang (Makino) Corner. Retrieved from, http://www.worldfloraonline.org/taxon/wfo-0000689924. [Accessed 20 October 2021].

[6] Stegmann P, Londo M, Junginger M. The circular bioeconomy: its elements and role in European bioeconomy clusters. Resour Conserv Recycl X 2020;6:100029.

[7] Liao CR, Kao CP, Peng WH, Chang YS, Lai SC, Ho YL. Analgesic and anti-inflammatory activities of methanol extract of *Ficus pumila* L. in mice. Evid Based Complementary Altern 2012:340141.

[8] Baird L, Yamamoto M. The molecular mechanisms regulating the KEAP1-NRF2 pathway. Mol Cell Biol 2020;40: e00099-20.

[9] Itoh K, Wakabayashi N, Katoh Y, Ishii T, Igarashi K, Engel JD, et al. Keap1 represses nuclear activation of antioxidant responsive elements by Nrf2 through binding to the amino-terminal Neh2 domain. Genes Dev 1999;13:76–86.

[10] Singh E, Swamy G, Matada P, Abbas N, Dhiwar PS, Ghara A, et al. Management of COVID-19-induced cytokine storm by Keap1-Nrf2 system: a review. Inflammopharmacology 2021; 29:1347–55.

[11] Pagadala NS, Syed K, Tuszynski J. Software for molecular docking: a review. Biophys Rev Lett 2017;9:91–102.

[12] Kong R, Yang G, Xue R, Liu M, Wang F, Hu J, et al. COVID-19 docking server: a meta server for docking small molecules, peptides and antibodies against potential targets of COVID-19. Bioinformatics 2020;36:5109–11.

[13] Wang M, Carver J, Phelan V, Sanchez LM, Garg N, Peng Y, et al. Sharing and community curation of mass spectrometry data with global natural products social molecular networking. Nat Biotechnol 2016;34:828–37.

[14] Ermanis K, Parkes KEB, Agback T, Goodman JM. Expanding DP4: application to drug compounds and automation. Org Biomol Chem 2016;14:3943–9.

[15] Hu HC, Li CY, Tsai YH, Yang DY, Wu YC, Hwang TL, et al. Secondary metabolites and bioactivities of *Aspergillus ochraceopetaliformis* isolated from *Anthurium brownie*. ACS Omega 2020;5:20991–9.

[16] Chiang CC, Korinek M, Cheng WJ, Hwang TL. Targeting neutrophils to treat acute respiratory distress syndrome in coronavirus disease. Front Pharmacol 2020; 11:572009.

[17] Ackermann M, Anders H, Bilyy R, Bowlin GL, Daniel C, Lorenzo RD, et al. Patients with COVID-19: in the dark-NETs of neutrophils. Cell Death Differ 2021;24:1–15.

[18] Crüsemann M, O'Neill EM, Larson CB, Melnik AV, Floros DJ, da Silva RR, et al. Prioritizing natural product diversity in a collection of 146 bacterial strains based on growth and extraction protocols. J Nat Prod 2017;80: 588–97.

[19] Robledinos-Antón N, Fernández-Ginés R, Manda G, Cuadrado A. Activators and inhibitors of NRF2: a review of their potential for clinical development. Oxid Med Cell Longev 2019:9372182.

[20] Kao YT, Chen YS, Tang KW, Lee JC, Tseng CH, Tzeng CC, et al. Discovery of 4-anilinoquinolinylchalcone derivatives as potential NRF2 activators. Molecules 2020;25:3133.

[21] Dong E, Du H, Gardner L. An interactive web-based dashboard to track COVID-19 in real time. Lancet Infect Dis 2020; 20:533–4.
[22] Coperchini F, Chiovato L, Ricci G, Croce L, Magri F, Rotondi M. The cytokine storm in COVID-19: further advances in our understanding the role of specific chemokines involved. Cytokine Growth Factor Rev 2021;58: 82–91.
[23] Ragab D, Eldin HS, Taeimah M, Khattab R, Salem R. The COVID-19 cytokine storm; what we know so far. Front Immunol 2020;11:1446.
[24] Hassanein EHM, Sayed AM, Hussein OE, Mahmoud AM. Coumarins as modulators of the Keap1/Nrf2/ARE signaling pathway. Oxid Med Cell Longev 2020:1675957.
[25] Abdelmohsen UR, Albohy A, Abdulrazik BS, Bayoumi SAL, Malak LG, Khallaf ISA, et al. Natural coumarins as potential anti-SARS-CoV-2 agents supported by docking analysis. RSC Adv 2021;11:16970–9.